PERGAMON

International Journal of Heat and Mass Transfer 44 (2001) 399–415

International Journal of HEAT and MASS TRANSFER

www.elsevier.com/locate/ijhmt

A study of bubble dynamics in reduced gravity forced-convection boiling

Yue Ma[a], J.N. Chung[b]

[a]School of Mechanical and Materials Engineering, Washington State University, Pullman, WA 99164-2920, USA
[b]Department of Mechanical Engineering, University of Florida, Gainesville, FL 32611-6300, USA

Received 12 December 1998; received in revised form 1 March 2000

Abstract

Experiments are reported in which a single vapor bubble was nucleated and grown in a flow field of FC-72 on a flat surface in terrestrial gravity and microgravity. A thin gold film semi-transparent heater was designed and used to generate single bubbles. Bubble nucleation, growth, and departure in microgravity with different flow rates were observed by a CCD camera. It was found that the transient bubble diameters during growth are proportional to the parameter of $(Re^{-1/3}t^{*1/3})$, where Re is the Reynolds number and t^* is the dimensionless time. The forced-convection would affect the downstream edge of a bubble significantly in microgravity, while the upstream coordinate of a bubble seems to be independent of the flow rate. It was observed that the high flow rate would offset the buoyancy effects. As a result, the bubble generation frequency, Weber number, and bubble shape tend to be similar with those in normal gravity.

1. Introduction

Forced-convection boiling has been recognized as one of the most efficient terrestrial heat transfer mechanisms [1,2]. In microgravity, forced-convection boiling has been found to be able to maintain this relatively high efficiency under certain flow conditions where bubble agglomeration was avoided [3,4]. Therefore, in this paper, we focus on the nucleation, growth, and departure of a single bubble in a flow field under microgravity. With this approach, we hope to gain a more fundamental understanding of the interaction mechanisms between a vapor bubble and its surrounding flow field in microgravity.

First we review the literature in the area of terrestrial bubble dynamics in forced-convection boiling. Among the early works, Levy [5] developed a correlation based on simple force balances for vapor bubble departure diameter in an upflow boiling of subcooled water. Koumoutsos et al. [6] investigated vapor bubble lift-off from an artificial nucleation site located on a horizontal heater surface with saturated water flowing over it. They observed that bubbles slide away from the nucleation site and continue to grow until lift-off. They also presented a correlation for lift-off diameters based on force balances. The buoyancy force was found to be an important parameter. Al-Hayes and Winterton [7] performed an extensive series of measurements to study vapor bubble diameters during detachment into flowing liquids. They used test liquids of water, water mixed with surface-active agent, and ethylene glycol. With different surfaces, equilibrium contact angles between the bubble and the heater surface ranging from 22° to 90° were obtained. In general, they found that the departure diameter decreased with increasing flow velocities. The departure diameters were a strong function of the contact angle.

0017-9310/01/$ - see front matter
PII: S0017-9310(00)00106-X

Nomenclature

A	center area of single bubble heater
A_b	bubble projected area from the side view
c_l	specific heat of liquid
D	bubble diameter
D^*	dimensionless bubble diameter
g	acceleration due to gravity
H	height of bubble
h_{fg}	latent heat of vaporization
I	current through the heater
Ja	Jacob number defined as $\rho_l c_l(T - T_{sat})/\rho_v h_{fg}$
L	length of heater
La	Laplace number
p_g	gas pressure
q''	nominal heat flux
q''_c	critical heat flux in terrestrial pool boiling
q''^*	dimensionless heat flux
Re	Reynolds number based on heater length
t	time
t^*	dimensionless time
T	temperature
T_{sat}	saturation temperature
U	mean bulk velocity of flow
V	voltage across the heater center
V'	dimensionless bubble volume assuming sphere shape
V^*	dimensionless bubble volume for deformed shape
We	Weber number based on departure diameter
Z	bubble position coordinate
Z^*	dimensionless bubble position coordinate

Greek symbols

ρ_l	liquid density
ρ_v	vapor density
σ	surface tension
ν	kinetic viscosity
γ_ρ	density ratio of liquid to vapor phase

Subscripts

b	bubble
c	critical
d	departure
l	liquid
sat	saturation
v	vapor

The departure diameters were measured to be of the order of 1 mm for contact angles of 22° and 28°, and of the order of 2 mm for contact angles of 82° and 90°. The important conclusion is that over a wide range of bubble Reynolds numbers the drag coefficient calculated from the local flow velocity is essentially at 1.22, regardless of different contact angles.

Klausner et al. [8] performed experiments of R113 forced-convection boiling over a horizontal heating surface. They observed that once a vapor bubble departs from its nucleation site, it typically slides along the heating surface and lifts-off at some finite distance downstream. They found that the measured departure diameter probability density functions (pdfs) showed a systematic dependence on the mass flow rate and heat flux. In general, an increase in the mass flow rate shifts the pdf curve towards lower departure diameters, and a decreased heat flux causes smaller departure diameter. They also presented an analytical force balance model that governs the bubble departure and lift-off. Analysis based on the model suggested that surface tension force alone could not prevent departure. The inertia of the liquid due to asymmetric bubble growth is important in holding the bubble at the nucleation site. An improved model (Zeng et al. [9]) was published by the same group of researchers shortly after the publication of Klausner et al. [8]. In [9], the inclination angle, which is defined as the angle between the major axis of the bubble and the vertical axis and is found to be important in the determination of the force due to bubble growth acting in the direction of flow, is determined on a dynamic basis and therefore is not required as input. Zeng et al. [9] also made an important assumption that the surface tension force is small compared to other forces acting on a vapor bubble at the moment of departure and lift-off. Thus, information on the experimentally measured bubble contact diameter and contact angle is not required. All of these make the model more independent of experimental data for fixing the parameters. They also provided a new set of data on mean bubble lift-off diameters for flow boiling of R113 on a nichrome heating strip. The predicted departure and lift-off diameters agreed well with their measured values.

Bibeau and Salcudean [10] also investigated forced-convection subcooled boiling using high-speed photography. They performed water boiling experiment in a vertical circular annulus for mean flow velocities of 0.08–1.2 m/s and subcooling of 10–60°C. They found that: (i) bubbles do not grow

and collapse on the heated wall, but eject into the flow for subcooling below 60°C; (ii) after onset of nucleate boiling, bubbles slide away from the nucleation site and later eject into the flow; (iii) bubbles condense while sliding on the heater wall; (iv) on the average, bubbles slide less than 2 mm, but it could be as long as 50 mm near the onset of nucleate boiling.

Recently Mei et al. [11,12] employed numerical analysis to study the vapor growth in heterogeneous boiling. They identified four dimensionless groups: Jacob number, Fourier number, thermal conductivity ratio, and thermal diffusivity ratio between the liquid and solid as the dominant parameters. The results provided first information on the transport mechanisms among vapor bubble, liquid microlayer, and heater surface.

Next, we review the bubble dynamics in microgravity. Cooper et al. [13] experimentally investigated the growth and departure of vapor bubbles on a vertical flat plate in a laminar upflow of supersaturated n-hexane. They performed the experiments in both normal gravity and microgravity. Bubbles were also found rolling on the heater surface in normal gravity. Cooper et al. [13] suggested that the simple models introduced by Levy [5] and Koumoutsos et al. [6] did not agree with their experimental data for bubble departure because [5] and [6] neglected the difference between the advancing and receding surface-to-bubble contact angles when modeling the surface tension force. Cooper et al. [13] introduced an empirical proportionality constant to account for this difference. From microgravity experiment, they concluded that bubble growth is merely dependent on the Jacob number defined as $\rho_l c_l(T - T_{sat})/\rho_v h_{fg}$ and liquid thermal diffusivity, with negligible influence of viscosity and surface tension. The only other work on forced-convection bubble dynamics in microgravity was reported by Wang et al. [3] and Ma and Chung [4]. Based on photographic results [3], they concluded that for a given heat flux level, if the flow velocity is higher than a threshold value, individual bubbles would slide and roll on the heater surface. On the average, the bubble velocities after departure from their nucleation sites ranged between 80 and 90% of the liquid free stream velocity. Ma and Chung [4] generated a boiling map to provide two-phase flow patterns as a function of the flow rate and heat flux. It was observed that the forced flow would decrease the average bubble size and increase the heat transfer coefficient.

The main purpose of this paper is to seek fundamental understanding of bubble dynamics in a forced-flow environment under microgravity. In order to achieve this goal, a special heater was designed and built to produce one bubble at a time.

2. Experimental apparatus

Experiments on forced-convection boiling and those of pool boiling to obtain the reference data were conducted in both earth gravity and reduced gravity. The reduced gravity environment was obtained in a 1s drop tower at Washington State University with an effective acceleration of the order of 10^{-3} g, which was measured by an accelerometer. The flow boiling apparatus consists of a pump, preheater, boiling test section, condenser, lighting, video, and data acquisition system (Fig. 1). The maximum free-stream velocity over the heater surface can reach up to 35 cm/s. According to the catalog information and calibration using a CCD video camera, the uncertainty of flow meter is $\pm 4\%$ full scale (± 1.4 cm/s), and the level of fluctuations during repeat tests is $\pm 1\%$ full scale (± 0.35 cm/s). In the experiment, the flow rate was varied from 6.5 to 30 cm/s. The temperature of the flow at the inlet of the test section was set at 30°C. Due to the heating from a running pump and a light bulb, the bulk temperature of the flow would fluctuate about ± 2°C during the experiment. The effect of this variation is negligible due to a relatively large degree of subcooling. In our study, the system was sealed from the surroundings and the system pressure was measured at 112 ± 3 kPa. The system pressure was higher than that of local atmosphere. This is because of the hydrostatic pressure head and the evaporation of working fluid. A visualization study was performed using a CCD camera with a frame rate of 1/30 s and a shutter speed of 1/1000 s.

In the experiment, FC-72, a Fluorinert, was chosen as the working fluid because it is clear, colorless, odorless, non-flammable, and non-explosive. This fluid also has the benefits of low toxicity, thermal and chemical stability, and compatibility with metals and plastics. However, because of the high solubility of dissolved gases in FC-72, degassing was necessary. We decided to perform the degassing by boiling and drawing a vacuum, which turned out to be quite effective. Before each experiment, we performed magnetic stirring while drawing vacuum for 15 min and then followed by constant boiling for 5 min. You et al. [14] reported a study on boiling incipience probability (the fraction of the total cases that successfully initiate nucleate boiling, for example, when the degree of superheat is raised to 24°C, two out of 10 cases have failed to boil, a probability of 80% is registered) for various dissolved gas pressures ($p_g = 3.6$, 50 and 104 kPa). For $p_g = 3.6$ kPa, their system is almost dissolved gas free. In Fig. 2, a comparison with the results of You et al. [14] for the incipient boiling probability shows that degas-

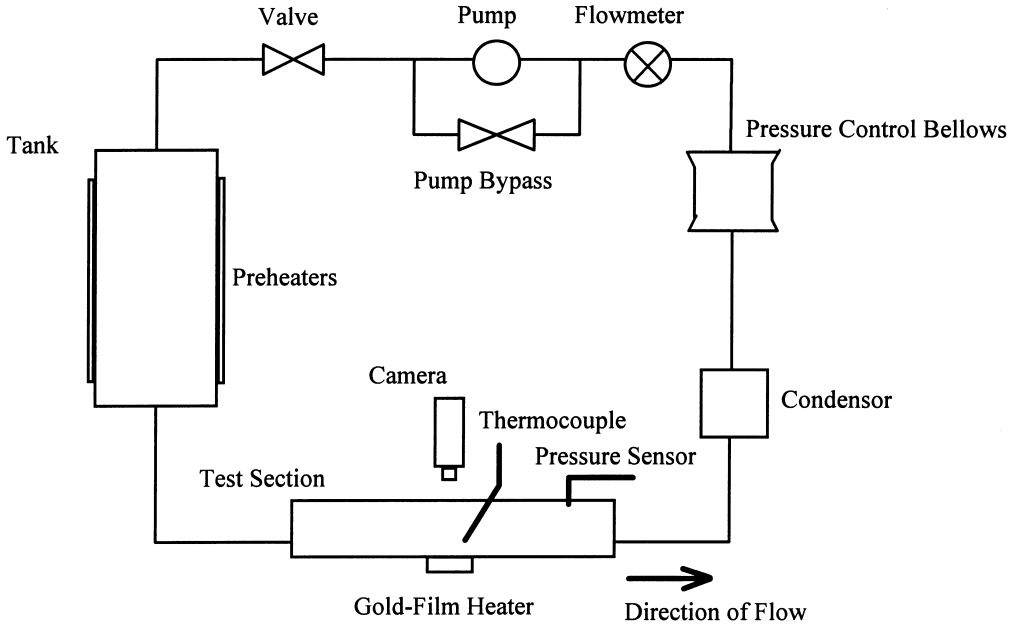

Fig. 1. Schematic of experimental system.

sing in a vacuum can efficiently remove the dissolved gas in the liquid. For $p_g = 3.6$ kPa, the dissolved gas in the liquid should be less than 0.0025 mole/mole. At the atmospheric condition, the boiling point of FC-72 is 56.3°C (3 M Manual). The boiling point of the fluid used in our experiment was measured at 56°C by a thermocouple. Therefore the degree of subcooling in the experiment was 26 ± 2°C.

The single-bubble heater was built by sputtering a 0.045 μm thick gold film on a piece of Pyrex glass, then annealing at 180°C for 3 h. Because the thin film can provide a suitable balance among specific resistance, temperature coefficient of resistance, and rapid response, the heater is ideal for the transient nucleate boiling studies under both terrestrial and microgravity conditions. In order to generate single bubbles, the center of heater was specially designed where the heating area was about 1 mm × 1 mm, as shown in

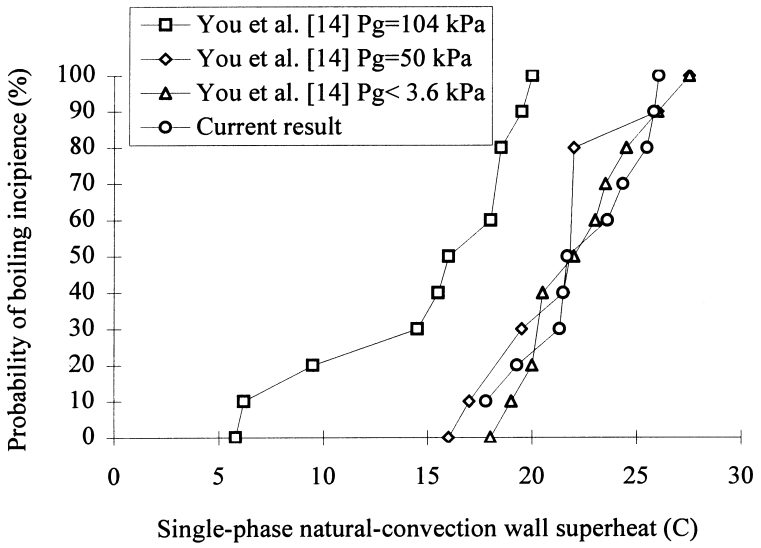

Fig. 2. Effect of dissolved gas on nucleate boiling inception.

Fig. 3(a). We found that any heater which is larger than the current heater size would tend to produce more than one bubbles at a time. Most of the correlations for bubble departure sizes predict that bubble departure sizes are around 1 mm. The copper tape or silver epoxy is used to connect the gold film to the copper lead which is tied to the power supply and A/D board. The nominal heat flux, which was defined as the heat flux provided by the heater center in earth gravity without forced convection, was estimated by the following:

$$q'' = \frac{I \cdot V}{A} \tag{1}$$

where I is the current through the heater, V is the voltage across the heater center, and A is the heater center area. In the experiment, two nominal heat fluxes (39667 and 5446 W/m^2) were selected with the uncertainty of $\pm$480 W/m^2. It is noted that the uncertainty for the heat flux measurement includes the heat loss to the substrate. The heat loss to the substrate was kept to minimum by turning on the heater only 3 s before the drop. Bubble size measurement was conducted using the "UTHSCSA Image Tool (version 1.28)" for Windows. This software is able to measure 1D or 2D quantities. In this study, the uncertainties in length and area are $\pm$0.5 mm and $\pm$0.3 mm^2, respectively.

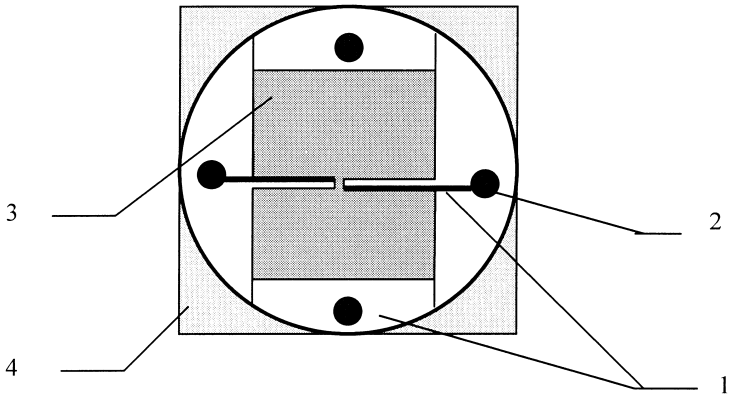

Fig. 3. Schematic of single bubble heater.

3. Experimental procedure

For each experiment, we first set up the required hardware and software for data acquisition. These included the video system and the airbag deceleration system of the drop tower. After setting the heat flux level and the flow rate using the calibration charts, the boiling system was hoisted up to the release position and the flow pump was turned on. The heater power was turned on only 3 s before the release in order to minimize the free-convection effects. It was determined that a 3 s heating period is long enough to establish a steady bubble generation pattern on the heater surface. Also, it was estimated that the free-convection effects established during the 3 s period would be convected downstream from the heater surface in 0.1–0.2 s for most of the flow rates in our experiment. Therefore, we believe the buoyancy effects are negligible in our microgravity experiment.

4. Results and discussion

In this study, the system parameters and results are presented in dimensionless forms and they are nondimensionalized as follows:

For nondimensional heat flux q''^*, we use the critical heat flux q''_c for terrestrial pool boiling on a large flat plate heater to nondimensionlize the heat flux.

$$q''^* = \frac{q''}{q''_c} \tag{2}$$

where q'' is dimensional heat flux and q''_c is the terrestrial pool boiling critical heat flux given in [15] as:

$$q''_c = 0.149 h_{fg} \sqrt{\rho_v} \sqrt[4]{g(\rho_l - \rho_v)\sigma} \tag{3}$$

where ρ_l, ρ_v, h_{fg}, σ, and g are the liquid density, vapor density, latent heat of vaporization, surface tension of the fluid, and the acceleration of earth gravity, respectively. The terrestrial critical heat flux is used as a common basis for comparison.

The velocity is non-dimensionalized by using the Reynolds number as follows:

$$Re = \frac{UL}{\nu} \tag{4}$$

where L is the length of heater, U is the mean bulk velocity of flow and ν is the kinetic viscosity of FC-72. In order to non-dimensionalize the length, the Laplace number La, which is used most frequently as a characteristic length in boiling, was selected in this study.

$$La = \sqrt{\frac{\sigma}{(\rho_l - \rho_v)g}} \tag{5}$$

In Figs. 12 and 14, the actual bubble diameter D and the upstream and downstream coordinate Z are all non-dimensionalized by La as follows:

$$D^* = \frac{D}{La} \tag{6}$$

$$Z^* = \frac{Z}{La} \tag{7}$$

To characterize the bubble shape, the aspect ratio of D/H is used in Fig. 12, where D is the horizontal length of the bubble and H is the vertical length.

4.1. Photographic visualization of bubble dynamics in terrestrial and microgravity

The images were obtained by a CCD camera with a frame rate of 1/30 s and a shutter speed of 1/1000 s. The typical bubble growth images under different conditions are shown in Figs. 4–9.

Fig. 4 shows the bubble growth process in pool boiling conditions under terrestrial gravity and microgravity. In terrestrial gravity, the bubble's shape evolved from a hemisphere to a spindle during the growth period. The contact area of the bubble with the heater would shrink with time as a result of necking due to the influence of buoyancy and surface tension, as shown in Fig. 4(a). In microgravity, bubble's shape developed from an oblate to nearly a sphere with the size larger than that in earth gravity, as shown in Fig. 4(b). The size is directly related to the rate of heating in microgravity. Our observation is, in general, consistent with the conclusion of Cooper and Chandratilleke [16].

Figs. 5, 6, and 7 show the images of bubble growth with a forced-flow condition in terrestrial gravity and microgravity for a higher heat flux ($q''^* = 0.432$) at various Reynolds number of 3645, 7850, and 16,821, respectively. In a flow field, the bubble shapes were no longer symmetrical due to the drag force on the bubble surface in the flow direction. In Figs. 5–7, the flow goes from right to left. It was found that the flow decreases the bubble size and increases the bubble inclination angle in both earth gravity and microgravity. The departure of bubbles from their nucleation sites in microgravity was observed and the increase of flow rate would shorten the time between the bubble birth and its departure from nucleation site. Observation of the bubble shapes for departure in reduced gravity revealed that the top of bubble would be bent in the flow direction for high Reynolds numbers. Based on Figs. 5–7, we found that the bubbles are generally larger and closer to the shape of a semi-sphere in microgravity. Bubbles are slenderer and taller in normal gravity. It is noted that at the highest flow rate

of $Re = 16{,}821$, the bubble size was seen to decrease after 0.07 s (Fig. 7(a)) instead of growth before departure for the lower flow rate cases. This is because convective heat loss from the bubble to the ambient flow exceeds the heat supplied from the heater. For reduced gravity at this highest flow rate, the bubble size and shape (Fig. 7(b)) differ from those at lower flow rates. They actually are similar to those of normal gravity, which suggests that gravity effects are negligible when forced convection is dominant.

Figs. 8 and 9 show the typical images of bubble growth in microgravity for a lower heat flux ($q''^* = 0.06$). In Fig. 8, the inclination angles of bubbles do not change much at a low flow rate ($Re = 3645$). Also, it was observed that bubbles slide along the heater surface after departure from the site of nucleation. When the flow rate was increased to $U = 20$ cm/s

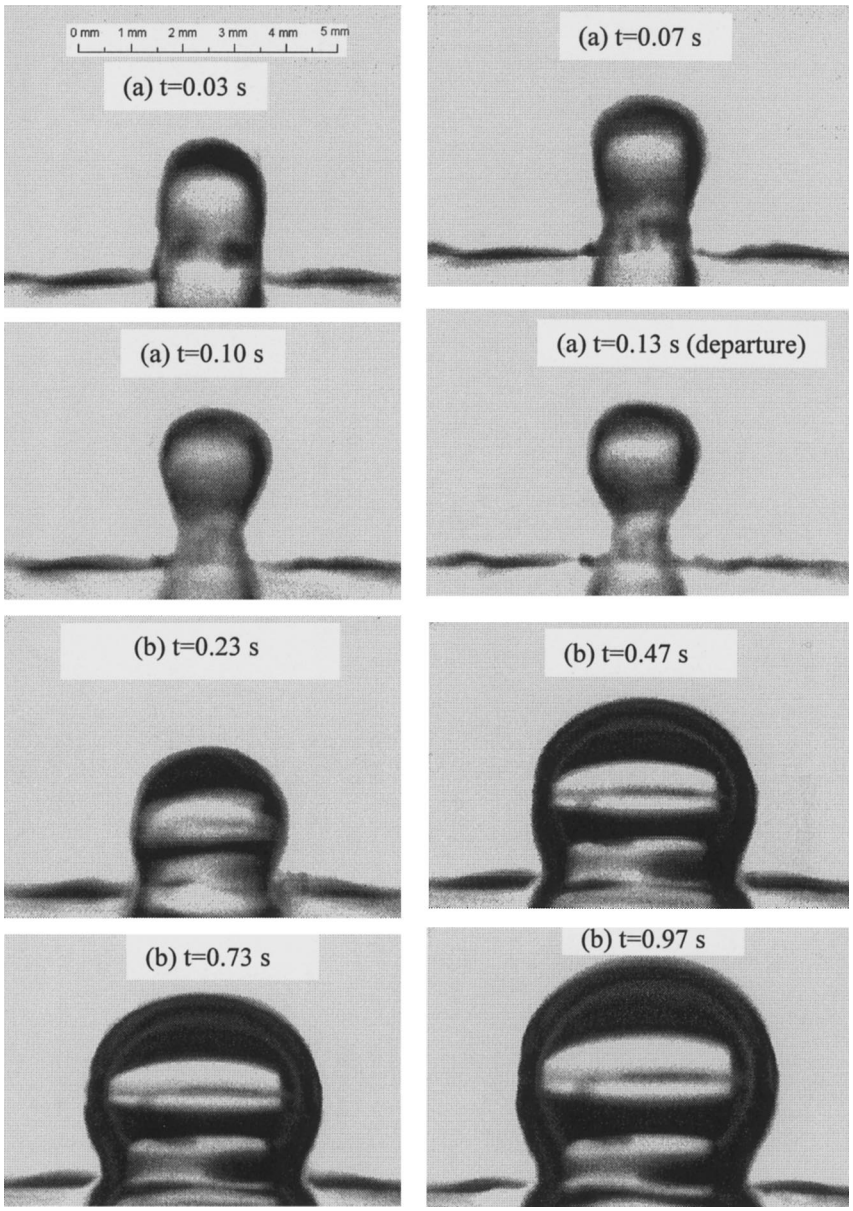

Fig. 4. Single bubble growth pool boiling (no forced-flow) with $q''^* = 0.432$: (a) normal gravity; (b) microgravity.

($Re = 11{,}214$), the size of the bubble decreased and the inclination angle increased, as shown in Fig. 9. When the flow rate reached $U = 30$ cm/s ($Re = 16{,}821$), it is interesting to note that no bubble nucleation is observed on the heater surface for the low heat flux case. The reason lies in the fact that the high flow takes away more heat from the surface, so that the heater was not able to maintain a high enough superheat for bubble nucleation to take place at a low heat flux. This is well known as "suppression of boiling".

4.2. Bubble growth phenomena for pool boiling in terrestrial gravity and microgravity

For pool boiling in microgravity, Straub et al. [17] conducted their experimental measurements using a flat surface heat flux-controlled heater with

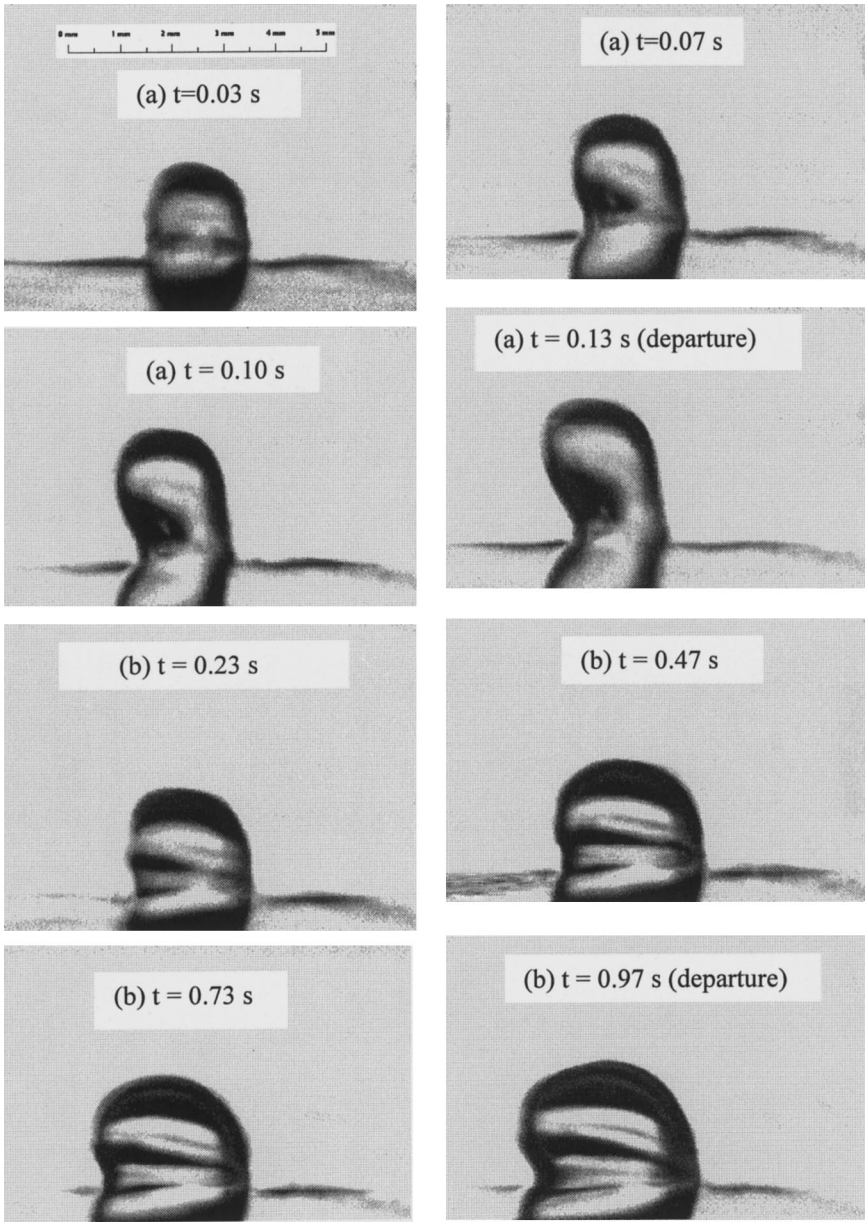

Fig. 5. Single bubble growth in forced-convection boiling for $Re = 3645$ with $q''^{*} = 0.432$: (a) normal gravity; (b) microgravity.

R-113 as the working fluid. With the same method and similar experimental conditions ($\Delta T_{sub} = 22$ K, $q'' = 42$ kW/m^2 in [17] and $\Delta T_{sub} = 26$ K, $q'' = 40$ kW/m^2 in current study), we compare our results of bubble size measurements with their published data in Fig. 10. The bubble radius is non-dimensionalized by the Laplace number, La. Nondimensional time t^* was defined as

$$t^* = \frac{q''}{La\rho_l h_{fg}} t \tag{8}$$

This dimensionless time reflects the effects of heat flux level, latent heat, and surface tension. It is noted that

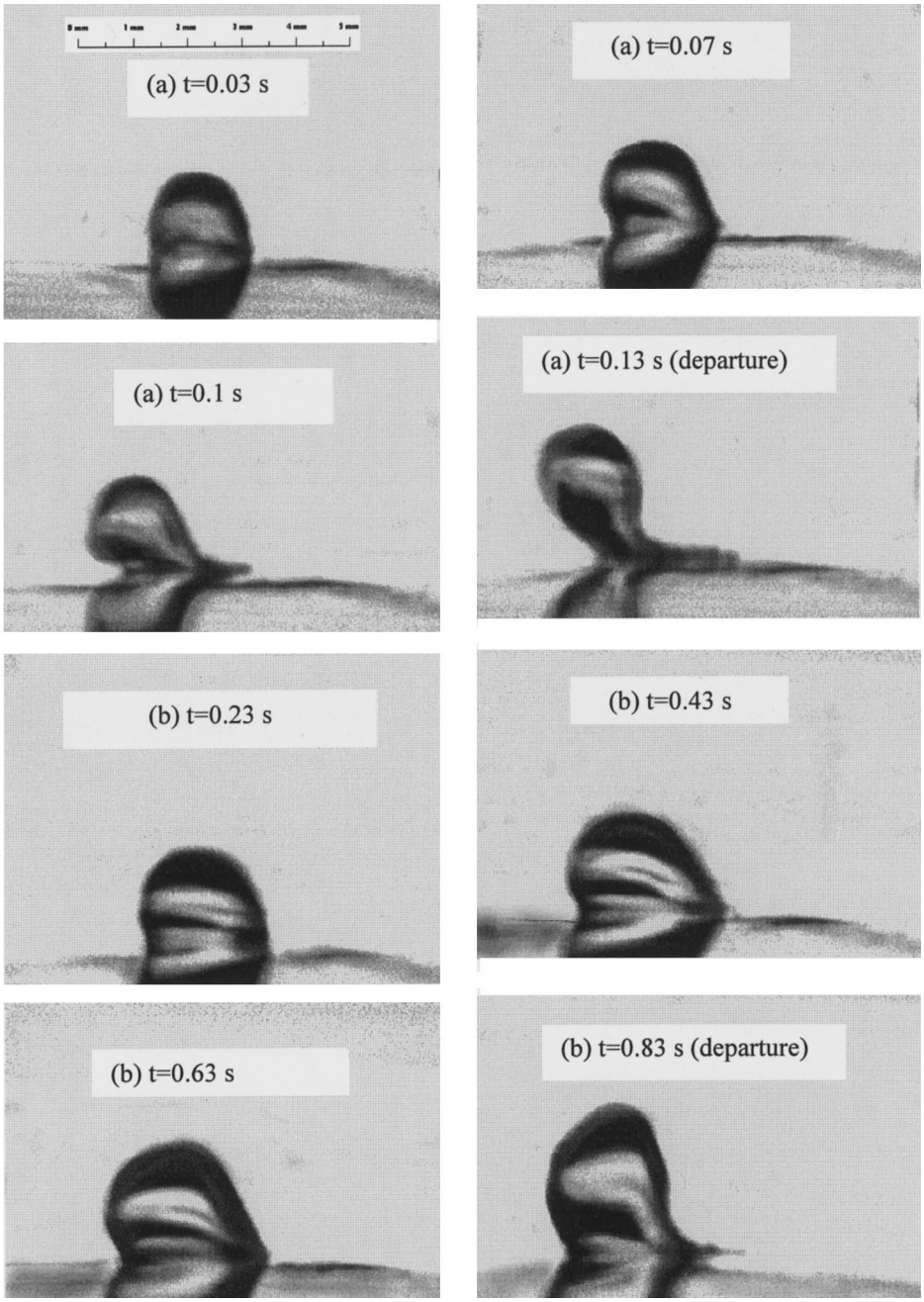

Fig. 6. Single bubble growth in forced-convection boiling for $Re = 7850$ with $q''^* = 0.432$: (a) normal gravity; (b) microgravity.

the time scale is based on terrestrial boiling conditions. In microgravity, there is no apparent time scale. We used the terrestrial scale to gain an insight in to the time process in microgravity relative to that on earth. Based on dimensionless quantities, our results agree closely with those of Straub et al. [17] for the length of time of their data. The close comparison also serves to verify our experimental system and data acquisition process.

A simplified model for bubble growth in microgravity pool boiling was developed based on thermal energy balance as given below:

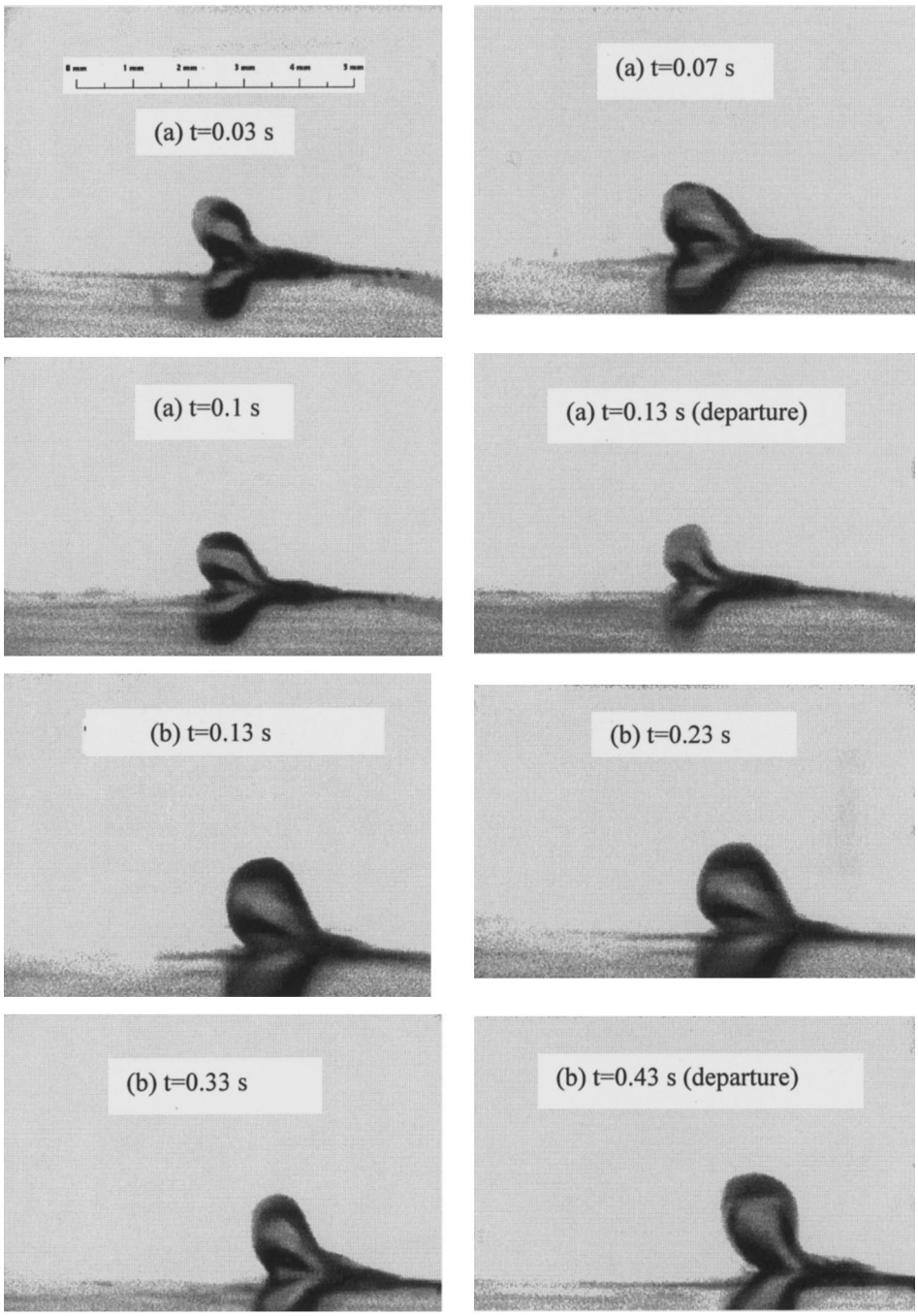

Fig. 7. Single bubble growth in forced-convection boiling for $Re = 16{,}821$ with $q''^{*} = 0.432$: (a) normal gravity; (b) microgravity.

$$\rho_v \frac{dV_v}{dt} = \frac{q''A}{h_{fg}} \tag{9}$$

where V_v is bubble volume and A is the heating area in contact with the base of the bubble. Applying the same dimensionless parameters as defined previously, the dimensionless form of Eq. (9) is as follows:

$$\frac{1}{A'}\frac{dV'}{dt^*} = \gamma_\rho \tag{10}$$

where $A' = A/La^2$ and $V' = V_v/La^3$. In the above, γ_ρ is the density ratio of liquid to vapor phase. Fig. 11 shows the current experimental data plotted according to Eq. (10). It is noted that for two different heat fluxes ($q''^* = 0.432$ and 0.06), Eq. (10) is able to collapse all the data around the constant value of γ_ρ. The success shown in Fig. 11 also supports the use of $\rho_l La h_{fg}/q''$ as the time scale.

A comparison of bubble shapes at two different heat fluxes in microgravity is shown in Fig. 12. It was found that the bubble shape would transform from an oblate to a sphere during the growth for both cases and a higher heat flux would cause the shape of bubbles to change faster, as indicated by the slopes of the curves.

4.3. The effects of forced convection on bubble growth in microgravity

The nominal volume of a bubble $(A_b)^{3/2}$ was selected

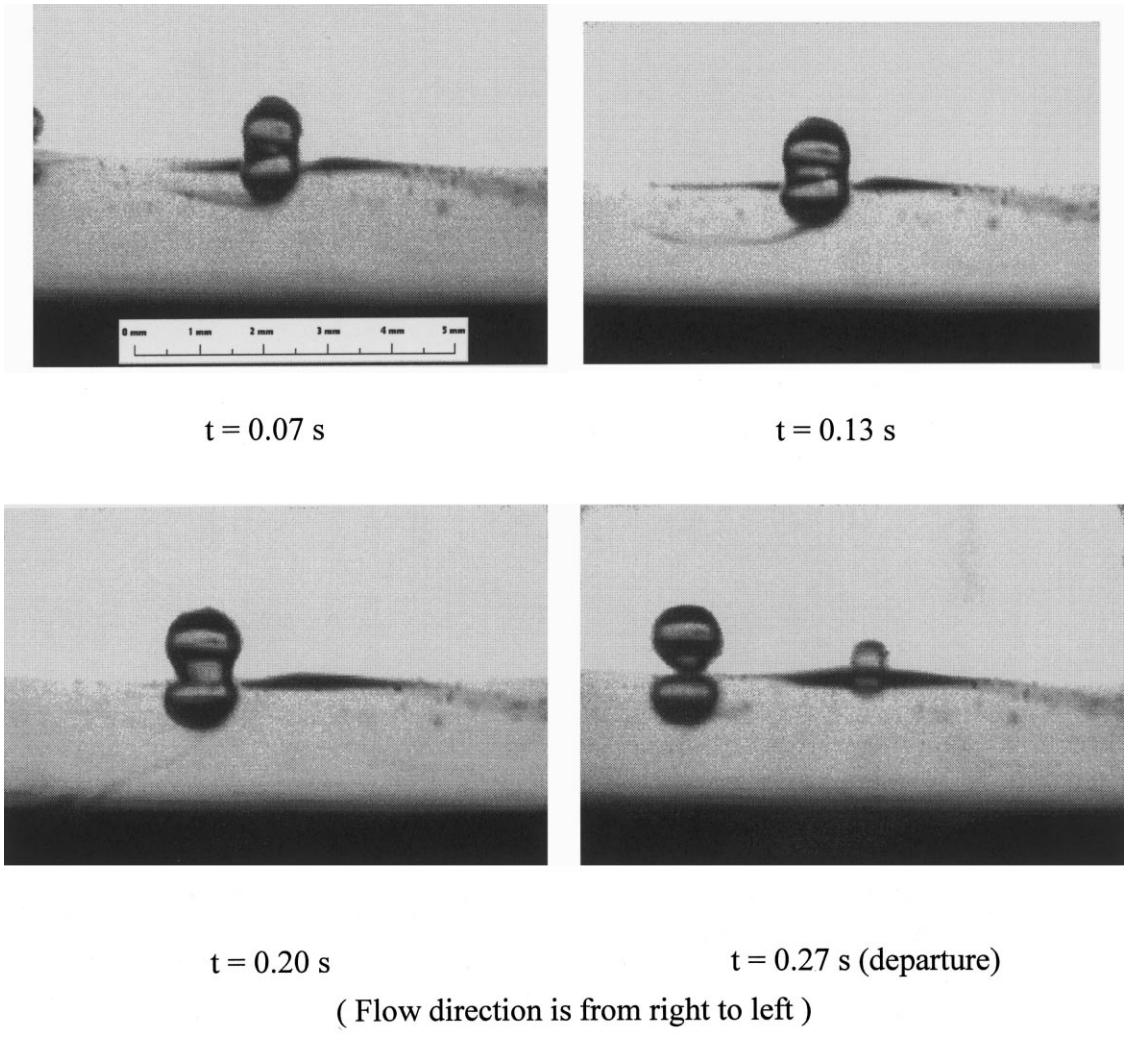

Fig. 8. Single bubble growth in microgravity forced-convection boiling for $Re = 3645$ with $q''^* = 0.06$.

as a simple parameter to correlate the growth of a bubble throughout its lifetime. Here A_b is the projected bubble area obtained from photographic measurement. The nondimensional nominal volume is taken to be:

$$V^* = \frac{(A_b)^{3/2}}{La^3} \tag{11}$$

Fig. 13 shows the bubble growth curves for various Reynolds numbers in microgravity. It was found that each curve could be approximated by a straight line without large errors except at initial stages. This provides a simple relationship between the bubble volume and the growth time. In other words, the diameter of a bubble during growth is proportional to one-third power of growth time ($D \propto t^{1/3}$). The slopes of the lines represent the bubble growth rates. In pool boiling, bubbles usually grow faster than those in flow boiling because the bubble heat loss to the surroundings would be much less. With the flow rate increased, the flow would take away more heat by convection from the bubble, which slows down the growth of the bubble. If we factor the effect of forced convection into the above relation, we can obtain the correlation of bubble growth in a flow field under microgravity. That is:

$$\frac{D}{La} = c_b Re^{-1/3} t^{*1/3} \tag{12}$$

Here c_b is a coefficient, which is a function of the liquid properties, heater properties, and bulk temperature. For FC72 with bulk temperature at 30°C, c_b is 28.3.

Forced convection also enhances the departure of bubbles from their nucleation sites. In our experiment, the bubbles were observed to depart at $t = 0.43$, 0.60, 0.83, and 0.97 s for Re = 16,821, 11,214, 7850, and

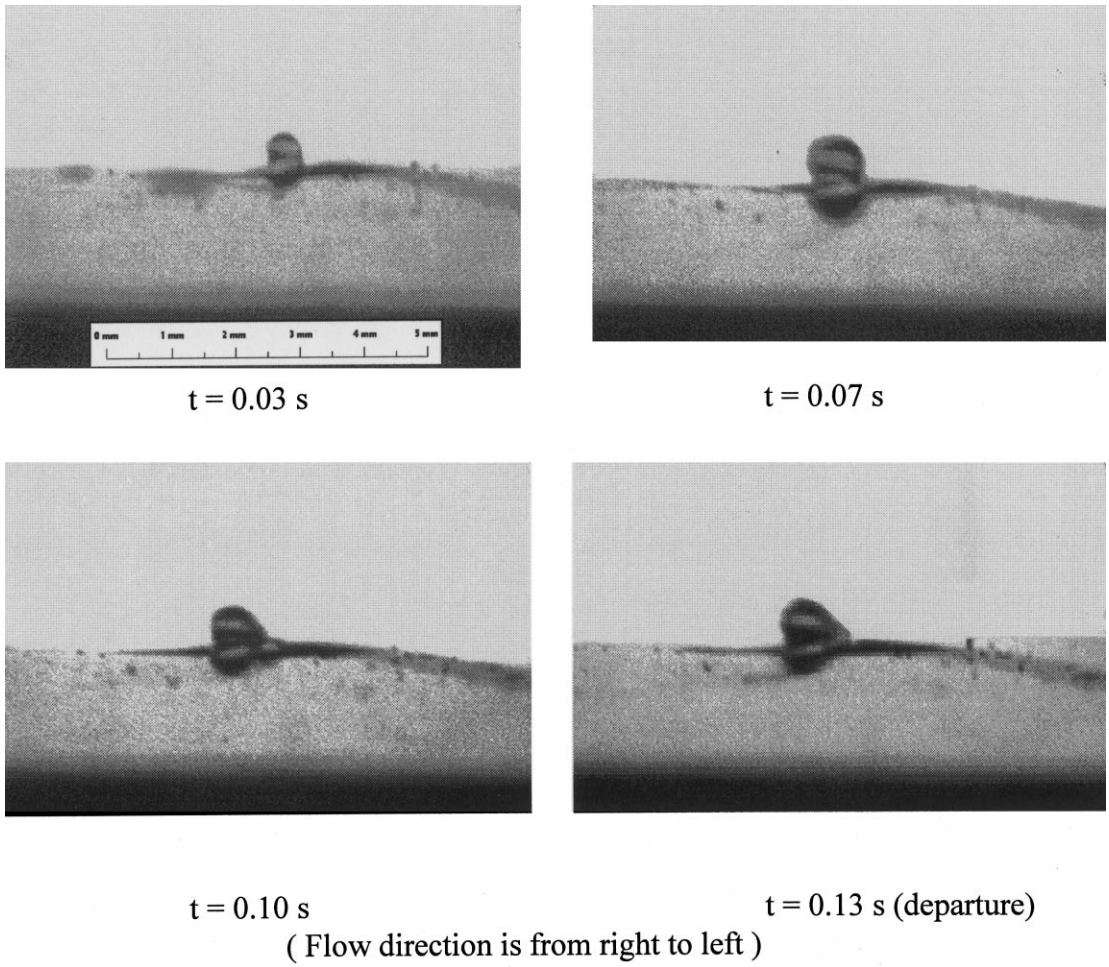

Fig. 9. Single bubble growth in microgravity forced-convection boiling for $Re = 11{,}214$ with $q''^* = 0.06$.

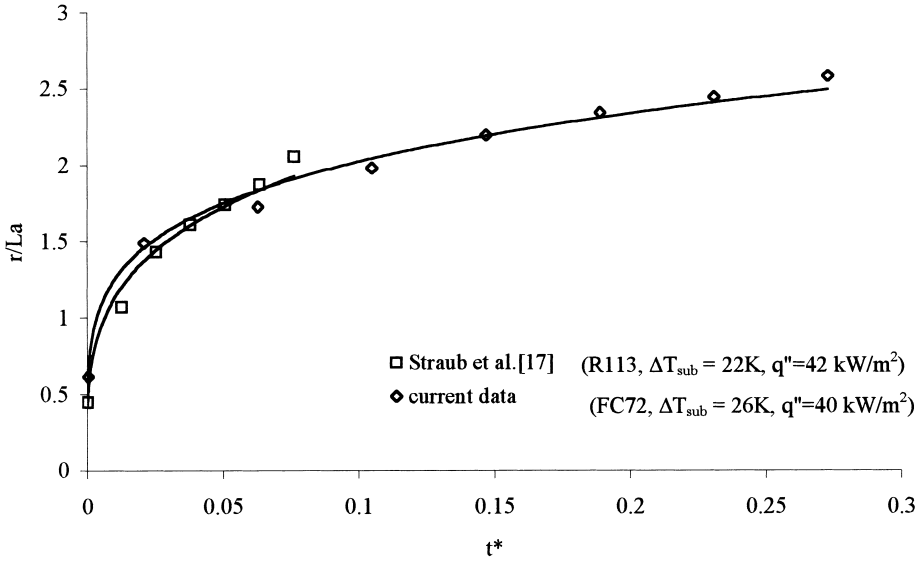

Fig. 10. Comparison of current data with published results on bubble growth rate in microgravity.

3645 for a high heat flux (q''^{*} = 0.432), respectively. The bubble in pool boiling was not observed to depart during the 1 s drop.

Fig. 14 shows the effects of forced convection and bubble growth on bubble upstream and downstream coordinates. At the initial stage of bubble growth, both upstream and downstream coordinates (absolute values) increase rapidly. During the growth of the bubbles, the downstream coordinates usually increase all the times. In contrast, the upstream coordinates increase in the beginning and then decrease slightly due to the drag force from the flow field. The effect of flow rates is also shown in Fig. 14. It was found that with the increase of flow rates, the bubbles' downstream coordinates decreased. However, the upstream coordinates of bubbles are almost independent of the flow rate. The above comparison is based on the maximum coordinates of the bubbles, which correspond to

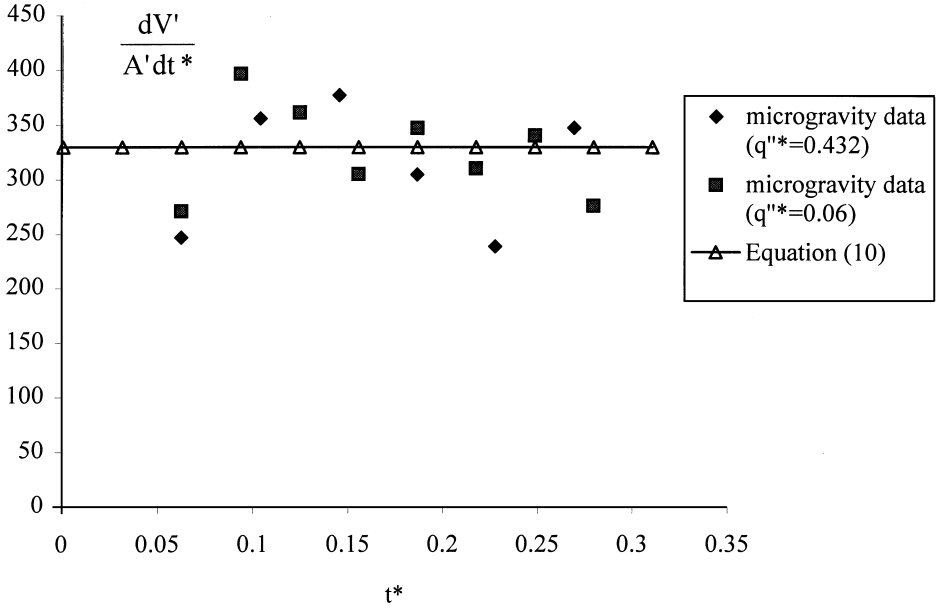

Fig. 11. Bubble size variation in microgravity without forced convection.

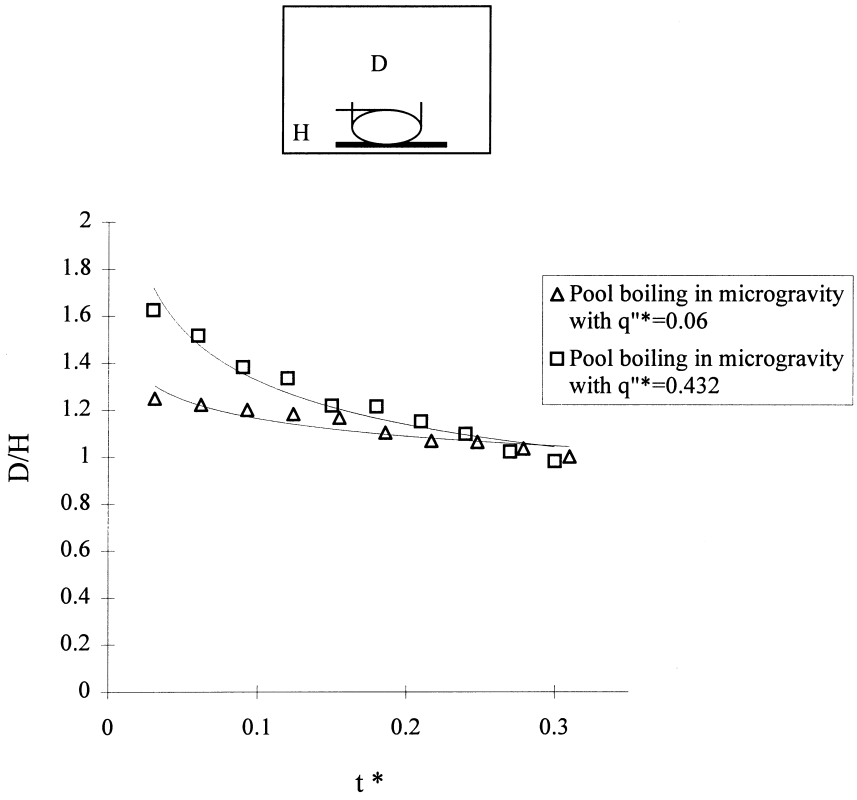

Fig. 12. Bubble shape variation in microgravity without forced convection.

those at the bubble departure. Fig. 15 shows that the forced convection flow in microgravity would tend to cause the bubble shapes to be similar after some time with the values of shape factor, D/H, close to unity in spite of the larger differences during initial stages. For the highest flow rate case ($Re = 16{,}821$), the shape factor did not change much during the growth of bubble, which implies that the shapes of bubble in microgravity might be similar during the growth period for the high flow rate forced-convection condition.

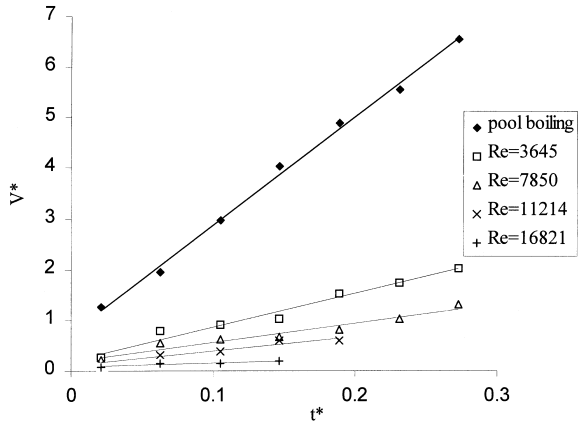

Fig. 13. The effect of forced convection on bubble growth in microgravity ($q''^* = 0.432$).

4.4. The effects of forced convection on bubble departure

In microgravity, the surface tension and liquid inertial forces dominate during the bubble departure process. Fig. 16 shows the relationship between departure diameter and flow rate for a high heat flux ($q''^* = 0.432$) in terrestrial gravity, a low heat flux ($q''^* = 0.06$) in terrestrial gravity and a high heat flux ($q''^* = 0.432$) in microgravity, respectively. The Weber number $We = \rho_l U^2 D_d/\sigma$ is used as a nondimensional measure of the bubble radius. It shows that the microgravity curve lies at the lowest due to the largest departure diameter of bubble in microgravity. A higher heat flux can also result in larger departure bubbles, so that the curve representing a higher flux case would locate lower than that for a lower heat flux case. It was noted that for high heat flux curves, no matter whether in terrestrial gravity or in microgravity, the curves tend to be close together as Reynolds numbers increase. Once the Reynolds number is greater than 10,000, the difference between any two curves is rela-

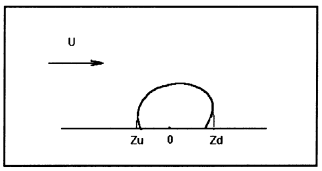

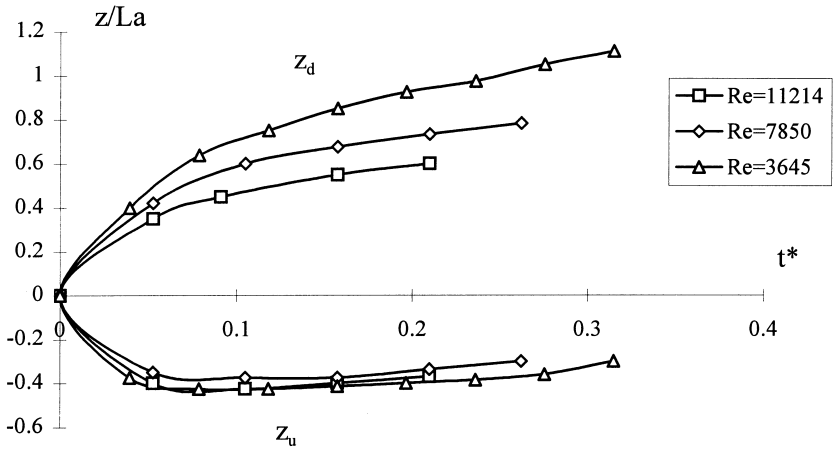

Fig. 14. The effect of forced convection on the upstream and downstream coordinates of bubbles in micrigravity ($q''^* = 0.432$).

tively small. This observation implies that the forced-flow would overpower effects caused by the buoyancy force.

Fig. 17 shows the effect of a flow field on the frequency of bubble generation for a low heat flux ($q''^* = 0.06$) in microgravity. It was found that the frequency of bubble generation increased with the increase in flow rate and the frequency in terrestrial

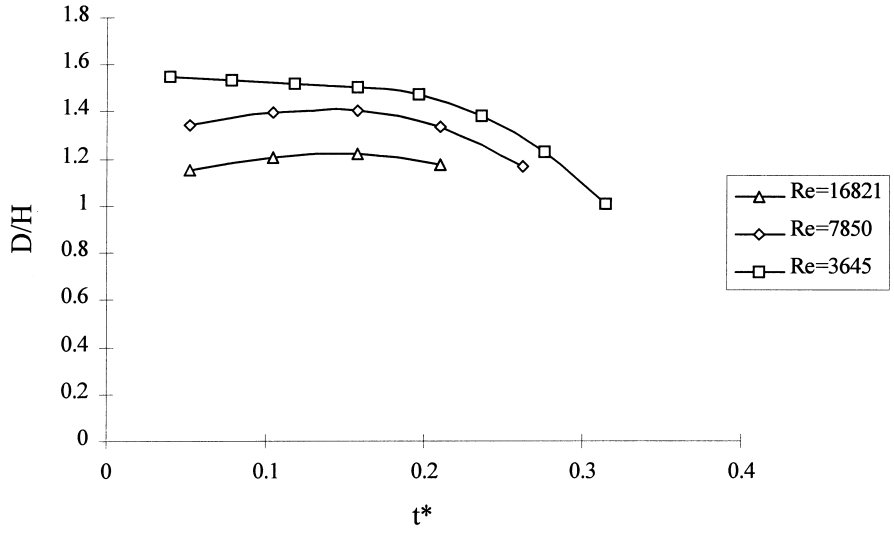

Fig. 15. The effect of forced convection on bubble shape in microgravity ($q''^* = 0.432$).

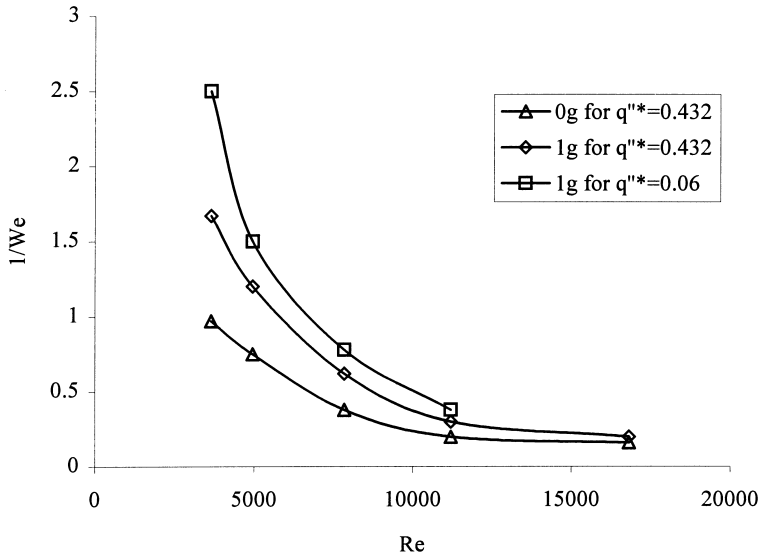

Fig. 16. The effect of heat flux and forced convection on bubble departure diameter.

gravity was higher than that in microgravity. However, the difference would tend to disappear if the Reynolds number is increased to 16,821. This phenomenon also shows that the high flow rate offsets the buoyancy effects.

This is all in a relative sense. In terrestrial gravity, buoyancy plays an important role in the bubble departure under pool boiling and low flow rates. In microgravity, bubble departure relies totally on the flow inertia. Therefore, at low flow rates the bubble departure process in terrestrial gravity is different from that in microgravity because of the terrestrial buoyancy. As the inertia increases due to increased flow rates, it is possible that above a high enough flow rate the flow inertia will dominate over the terrestrial gravity, which makes the bubble departure process on earth similar to that in microgravity.

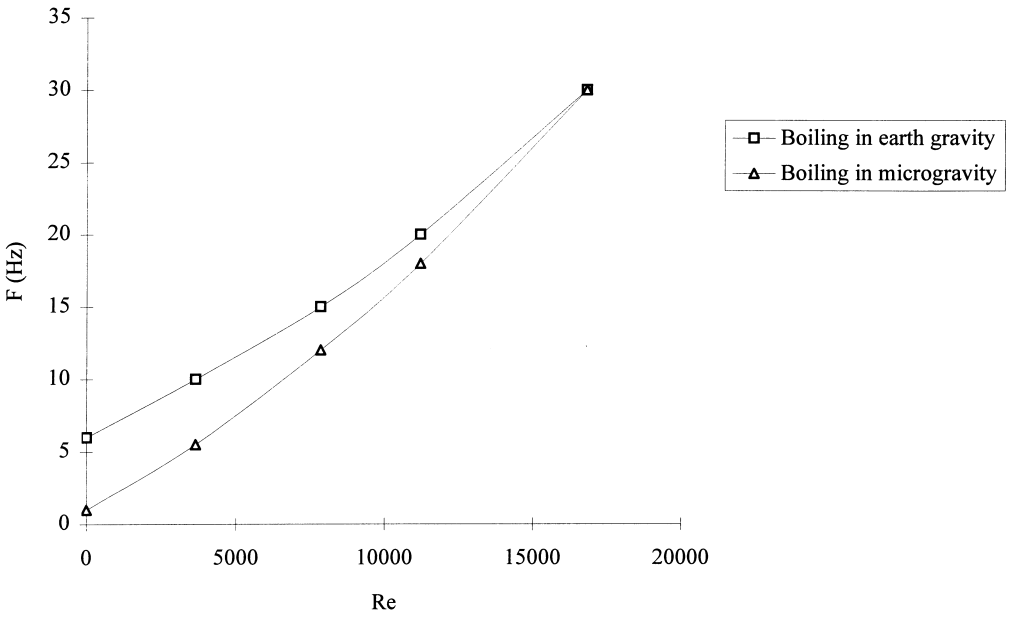

Fig. 17. The effect of forced convection on bubble generation frequency in microgravity with $q''^{*} = 0.06$.

5. Conclusion

1. In normal gravity, the bubble shape for pool boiling changes from a hemisphere to a spindle. The contact area shrinks as the bubble grows due to the effect of buoyancy. In microgravity, the bubble shape for pool boiling would stay as hemispherical and the size is much larger than that in normal gravity.
2. Once the flow rate is increased, the bubble departs earlier and the size of bubble decreases accordingly. When the flow rate is high enough, the boiling nucleation in both earth gravity and microgravity would disappear at a lower heat flux. The reason lies in the fact that the high flow rate takes away more heat from the surface so that the heater was not able to achieve the minimum superheat for nucleation.
3. In our experiment, it was found that the bubble growth diameter in a flow field under microgravity is proportional to the parameter of $(Re^{-1/3}t^{*1/3})$.
4. The forced-convection affects the downstream edge coordinate of a bubble significantly in microgravity. However, the upstream edge coordinate of a bubble seems to be flow rate independent in reduced gravity.
5. It was observed that the high flow rate would offset the microgravity effects. As a result, the bubble generation frequency, Weber number, and bubble shape tend to be similar to those in normal gravity at high flow rates.

Acknowledgements

This material is based on work supported by NASA under Grant No. NAG3-1387 and Dr. Fran Chiaramonte was the grant monitor, who provided constant support to our project.

References

[1] G. Tsung-Chang, S.G. Bankoff, On the mechanism of forced-convection subcooled nucleate boiling, Journal of Heat Transfer 112 (1990) 213–218.
[2] S.G. Bankoff, Future direction in two-phase and heat transfer in space. Keynote paper, in: Proceedings of Second Microgravity Fluid Physics Conference, 1994, pp. 3–11.
[3] T.C. Wang, T.J. Snyder, J.N. Chung, Experimental examination of forced-convection subcooled nucleate boiling and its application in microgravity, Journal of Heat Transfer 118 (1996) 237–241.
[4] Y. Ma, J.N. Chung, An experimental study of forced convection boiling in microgravity, Int. J. Heat Mass Transfer 15 (1998) 2371–2382.
[5] S. Levy, Forced convection subcooled boiling-prediction of vapor volumetric fraction, Int. J. Heat Mass Transfer 10 (1967) 951–965.
[6] N. Koumoutsos, R. Moissis, A. Spyridonos, A study of bubble departure in forced-convection boiling, Journal of Heat Transfer 90 (1968) 223–230.
[7] R.A.M. Al-Hayes, R.H.S. Winterton, Bubble diameter on detachment in flowing liquids, Int. J. Heat Mass Transfer 24 (1981) 223–230.
[8] J.F. Klausner, R. Mei, D.M. Bernhard, L.Z. Zeng, Vapor bubble departure in forced convection boiling, Int. J. Heat Mass Transfer 36 (1993) 651–662.
[9] L.Z. Zeng, J.F. Klausner, D.M. Bernhard, R. Mei, A unified model for the prediction of bubble detachment diameters in boiling systems — II. Flow boiling, Int. J. Heat Mass Transfer 36 (1993) 2271–2279.
[10] E.L. Bibeau, M. Salcudean, A study of bubble ebullition in forced-convective subcooled nucleate boiling at low pressure, Int. J. Heat Mass Transfer 37 (1994) 2245–2259.
[11] R. Mei, W. Chen, J.F. Klausner, Vapor bubble growth in heterogeneous boiling — I. Formulation, Int. J. Heat Mass Transfer 38 (1995) 909–919.
[12] R. Mei, W. Chen, J.F. Klausner, Vapor bubble growth in heterogeneous boiling — II. Growth rate and thermal fields, Int. J. Heat Mass Transfer 38 (1995) 921–934.
[13] M.G. Cooper, K. Mori, C.R. Stone, Behaviour of vapor bubbles growing at a wall with forced flow, Int. J. Heat Mass Transfer 26 (1983) 1489–1507.
[14] S.M. You, T.W. Simon, A. Bar-Cohen, Y.S. Hong, Effects of dissolved gas content on pool boiling of a highly wetting fluid, Journal of Heat Transfer 117 (1995) 687–692.
[15] J.H. Lienhard, V.K. Dhir, Hydrodynamic prediction of peak pool-boiling heat fluxes from finite bodies, Journal of Heat Transfer 95 (1973) 152–158.
[16] M.G. Cooper, T.T. Chandratilleke, Growth of diffusion-controlled vapor bubbles at a wall in a known temperature gradient, Int. J. Heat and Mass Transfer 9 (1981) 1475–1492.
[17] J. Straub, M. Zell, B. Vogel, Pool boiling in a reduced gravity field, Heat Transfer, Proceedings of 9th Int. Heat Transfer Conference 1 (1990) 91–112.